Lattice kinetic simulations in three-dimensional magnetohydrodynamics

G. Breyiannis* and D. Valougeorgis

Department of Mechanical and Industrial Engineering, University of Thessaly, Pedion Areos, Volos, 38333, Greece

(Received 23 January 2004; published 11 June 2004)

A lattice kinetic algorithm to simulate three-dimensional (3D) incompressible magnetohydrodynamics is presented. The fluid is monitored by a distribution function, which obeys a scalar kinetic equation, subject to an external force due to the imposed magnetic field. Following the work of Dellar [J. Comput. Phys. **179**, 95 (2002)], the magnetic field is represented by a different three-component vector distribution function, which obeys a corresponding vector kinetic equation. Discretization of the 3D phase space is based on a 19-bit scheme for the hydrodynamic part and on a 7-bit scheme for the magnetic part. Numerical results for magnetohydrodynamic (MHD) flow in a rectangular duct with insulating and conducting walls provide excellent agreement with corresponding analytical solutions. The scheme maintains in all cases tested the MHD constraint $\nabla \cdot \mathbf{B} = 0$ within machine round-off error.

I. INTRODUCTION

Lattice Boltzmann methods (LBM's) have been implemented in many areas of fluid flows [1]. They have been proven to be an efficient alternative to classical CFD solvers in incompressible low-Reynolds-number flows in complex geometries, including porous media and particulate-suspension multiphase flows [2]. They focus on the proper time, space, and microscopic particle velocity discretization of the mesoscopic Bhatnager-Gross-Krook (BGK) kinetic equation, in order to provide exact Lagrangian-type solutions, subject to specific conservation rules that reflect the macroscopic processes. Then, the corresponding macroscopic behavior is recovered at the long-wavelength limit. The explicit and local nature of the algorithm is amenable to high parallelization.

LBM's have been also applied in the field of two-dimensional (2D) magnetohydrodynamics (MHD). The first attempts were considered in the context of a second base vector for the discrete particle velocities on an hexagonal lattice [3,4]. Thus, for a lattice with N streaming directions, $N \times N$ particle states must be considered and as a result vast amounts of memory are required. This model has been simplified by implementing only adjacent auxiliary vectors for each lattice direction, while all other desired properties of the model have been retained [5]. This approach has also been extended in an octagonal lattice, due to its superior numerical stability properties compared to the hexagonal or square lattices [6,7]. However, despite significant efforts to reduce the complexity of the lattice MHD system, the applied multispeed formulation of the momentum and magnetic fields adds a significant burden on the numerics, suggesting a cumbersome extension to 3D geometry.

Recently, a new approach was proposed by Dellar [8]. The magnetic field is represented by a separate vector distribution function, which obeys a kinetic BGK-type evolution equation. Although there is no analogous microscopic process for the magnetic field, it can be argued that any conservative system can be formulated in this way under appropriate constrains [9]. Furthermore, the fluid momentum field is simulated via a typical BGK lattice equation. This formulation contains certain important advantages compared to the earlier multi-speed models (i.e., significantly reduced computer memory and independent adjustment of the fluid viscosity and magnetic diffusivity).

There are a number of ways to include the effects of the Lorentz force into the MHD formulation. Dellar opted for the heuristic extension of the equilibrium function that would induce an appropriate term to the second moment of the distribution function and thus to the momentum equation. A more systematic and general approach is based on the *a priori* derivation of the BGK equation with an external acceleration term included due to the imposed external potential [10–12]. Then the Lorentz force can be introduced as a pointwise force. It is noted that within this formulation the discretized expanded equilibrium retains the same form as in the hydrodynamic configuration.

In the present work, we apply the lattice kinetic scheme introduced by Dellar for the treatment of the induction equation to three-dimensional MHD flows. However, we choose to implement the more formal approach based on the extended Boltzmann equation in order to model the external Lorentz force term. Following this procedure the integrated scheme becomes more flexible and straightforward in its formulation.

II. FORMULATION

We start our analysis by noting that the proposed lattice scheme simulates the incompressible MHD flow equations, which consist of the momentum equation augmented by the Lorenz force

$$\partial_t(\varrho \mathbf{u}) + \nabla \cdot (P\mathbf{I} + \varrho \mathbf{uu}) = \mathbf{J} \times \mathbf{B} + \nabla \cdot (2\nu \varrho \mathbf{S}) \qquad (1)$$

and the induction equation, which in conservative form, can be written as

---

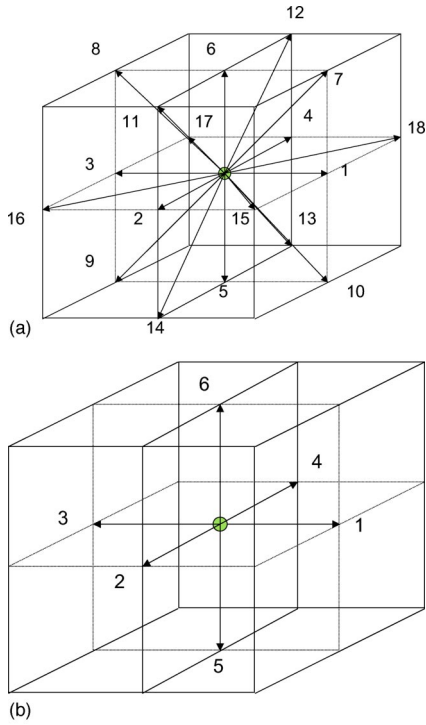*Corresponding author. Electronic address: gbregian@mie.uth.gr

FIG. 1. Discrete velocity lattice for the (a) hydrodynamic (3DQ19) and (b) magnetic (3DM7) fields.

$$\partial_t \boldsymbol{B} + \boldsymbol{\nabla} \cdot (\boldsymbol{u}\boldsymbol{B} - \boldsymbol{B}\boldsymbol{u}) = \eta \nabla^2 \boldsymbol{B}. \qquad (2)$$

Here, ϱ is the density, $\boldsymbol{u}$ and $\boldsymbol{B}$ denote the velocity and magnetic fields, respectively, $\boldsymbol{S}$ represents the strain rate tensor, $\boldsymbol{J}$ is the current density, and ν and η are the kinetic viscosity and magnetic resistivity. In addition, the solenoidal constrains of $\boldsymbol{\nabla}\cdot\boldsymbol{u}=0$, and $\boldsymbol{\nabla}\cdot\boldsymbol{B}=0$ are imposed.

At the mesoscale level, the flow can be monitored through the time and space evolution of a distribution function $f(\boldsymbol{x},\boldsymbol{\xi},t)$ which follows the BGK kinetic equation including the external forcing term,

$$\partial_t f + \boldsymbol{\xi} \cdot \boldsymbol{\nabla} f + \boldsymbol{a} \cdot \boldsymbol{\nabla}_{\xi} f = -(1/\lambda)(f - f^{eq}), \qquad (3)$$

where $\boldsymbol{\xi}$ and $\boldsymbol{a}$ stand as the particle velocity and acceleration, respectively, λ is the relaxation time, and f^{eq} is the local Maxwellian [12,13]. The acceleration is due to an imposed mean external potential and, under the MHD formulation,
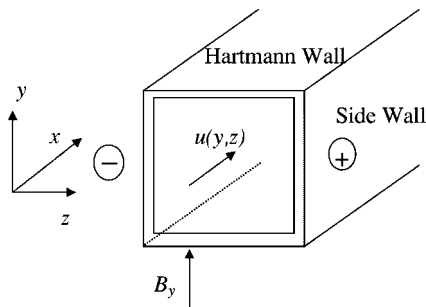

FIG. 2. Configuration of duct flow under an initial magnetic field $\boldsymbol{B}=(0,B_y,0)$.

relates to the Lorenz force $\boldsymbol{J}\times\boldsymbol{B}$. Equation (3) is integrated along its characteristic using the trapezoidal rule [11,12], while the unknown forcing term is treated according to the procedure in [10–12]. Note that considering a nonconstant acceleration during the integration step is appropriate due to the nature of the Lorenz force. Thus, the discrete distribution function $f_i(\boldsymbol{x},\boldsymbol{\xi}_i,t)$ satisfies the evolution equation

$$f_i(\boldsymbol{x} + \boldsymbol{\xi}_i\delta t, \boldsymbol{\xi}_i, t + \delta t) - f(\boldsymbol{x},\boldsymbol{\xi}_i,t)$$

$$= -\frac{\delta t}{2\tau}[f(\boldsymbol{x} + \boldsymbol{\xi}_i\delta t, \boldsymbol{\xi}_i, t + \delta t) - f^{(0)}(\boldsymbol{x} + \boldsymbol{\xi}_i\delta t, \boldsymbol{\xi}, t + \delta t)]$$

$$- \frac{\delta t}{2\tau}[f(\boldsymbol{x},\boldsymbol{\xi}_i,t) - f^{(0)}(\boldsymbol{x},\boldsymbol{\xi}_i,t)]$$

$$+ \frac{\delta t}{2}\boldsymbol{a}(\boldsymbol{x} + \boldsymbol{\xi}_i\delta t, \boldsymbol{\xi}_i, t + \delta t) \cdot \boldsymbol{\nabla}_{\xi_i} f(\boldsymbol{x} + \boldsymbol{\xi}_i\delta t, \boldsymbol{\xi}_i, t + \delta t)\delta t$$

$$+ \frac{\delta t}{2}\boldsymbol{a}(\boldsymbol{x},\boldsymbol{\xi}_i,t) \cdot \boldsymbol{\nabla}_{\xi_i} f(\boldsymbol{x},\boldsymbol{\xi}_i,t)\delta t, \qquad (4)$$

where δt denotes the time step, $\tau = \lambda/\delta t$ is the dimensionless relaxation time,

$$f_i^{(0)} = \varrho w_i \left[1 + \frac{(\boldsymbol{\xi}_i \cdot \boldsymbol{u})}{\theta} + \frac{(\boldsymbol{\xi}_i \cdot \boldsymbol{u})^2}{2\theta^2} - \frac{u^2}{2\theta} \right], \qquad (5)$$

and

$$\boldsymbol{a} \cdot \boldsymbol{\nabla}_{\xi_i} f_i = -\frac{w_i\varrho}{\theta^2}\left[(\boldsymbol{\xi}_i - \boldsymbol{u}) + \frac{(\boldsymbol{\xi}_i \cdot \boldsymbol{u})}{\theta^2}\boldsymbol{\xi}_i\right] \cdot (\boldsymbol{J}\times\boldsymbol{B}). \qquad (6)$$

In the present work, weights w_i and discrete velocities $\boldsymbol{\xi}_i$ reflect the 3DQ19 configuration [Fig. 1(a)], arguably the most efficient lattice for 3D computations [14], with $\nu = \tau\theta\delta t$. Setting the lattice speed $c=1$, for computational efficiency, we postulate $\theta = c_s^2 = 1/3$. The hydrodynamic macroscopic quantities are given as $\varrho = \Sigma_{i=0}^{18} f_i$, $\varrho\boldsymbol{u} = \Sigma_{i=0}^{18} \boldsymbol{\xi}_i f_i$.

Next, following the work of Dellar [8], we use a three-component vector distribution function $\boldsymbol{g}(\boldsymbol{x},\boldsymbol{\zeta},t)$, the zeroth moment of which gives the magnetic field vector $\boldsymbol{B} = \int\boldsymbol{g}d\boldsymbol{\zeta}$. The evolution of $\boldsymbol{g}$ obeys a kinetic equation of the form

$$\partial_t \boldsymbol{g} + \boldsymbol{\zeta} \cdot \boldsymbol{\nabla}\boldsymbol{g} = -(1/\lambda_m)(\boldsymbol{g} - \boldsymbol{g}^{(0)}), \qquad (7)$$

where $\boldsymbol{g}^{(0)}$ is the corresponding equilibrium distribution function and $\lambda \neq \lambda_m$ denotes a relaxation time, providing a second degree of freedom in the model. Equation (7) is integrated using the trapesoidal rule, yielding, in its discrete form, the evolution equation

$$\boldsymbol{g}_j(\boldsymbol{x} + \boldsymbol{\zeta}_j\delta t, \boldsymbol{\zeta}_j, t + \delta t) - \boldsymbol{g}_j(\boldsymbol{x},\boldsymbol{\zeta}_j,t)$$

$$= -\frac{\delta t}{2\tau_m}[\boldsymbol{g}_j(\boldsymbol{x} + \boldsymbol{\zeta}_j\delta t, \boldsymbol{\zeta}_j, t + \delta t) - \boldsymbol{g}_j^{(0)}(\boldsymbol{x} + \boldsymbol{\zeta}_j\delta t, \boldsymbol{\zeta}_j, t + \delta t)]$$

$$- \frac{\delta t}{2\tau_m}[\boldsymbol{g}_j(\boldsymbol{x},\boldsymbol{\zeta}_j,t) - \boldsymbol{g}_j^{(0)}(\boldsymbol{x},\boldsymbol{\zeta}_j,t)], \qquad (8)$$

where $\boldsymbol{g}_j(\boldsymbol{x},\boldsymbol{\zeta}_j,t)$ is the discrete-vector-valued distribution, $\tau_m = \lambda_m/\delta t$, and the discrete equilibrium takes the form
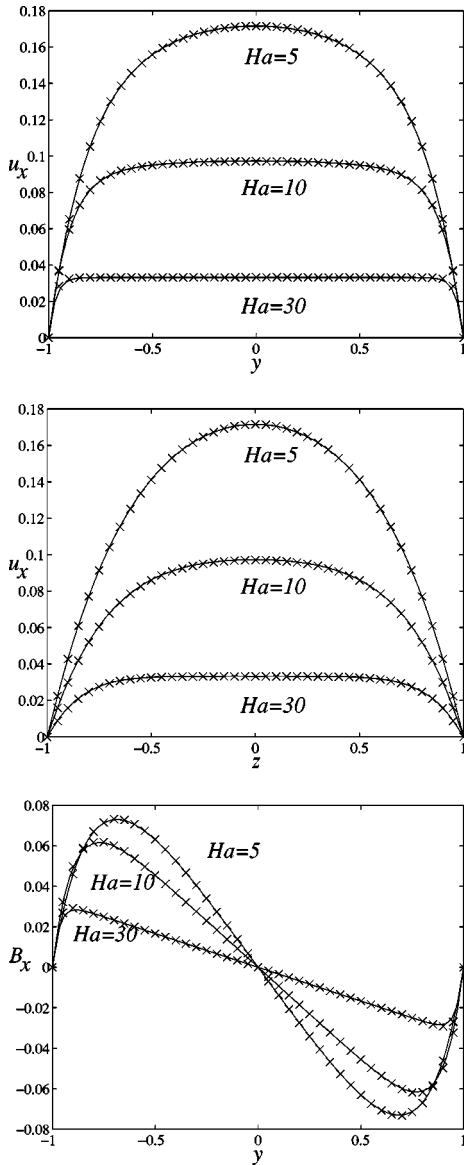
FIG. 3. Velocity profiles and induced magnetic field for various Ha numbers for the case of insulating side and Hartmann walls. Comparison between analytical (solid line) and computational ($\times$) results.
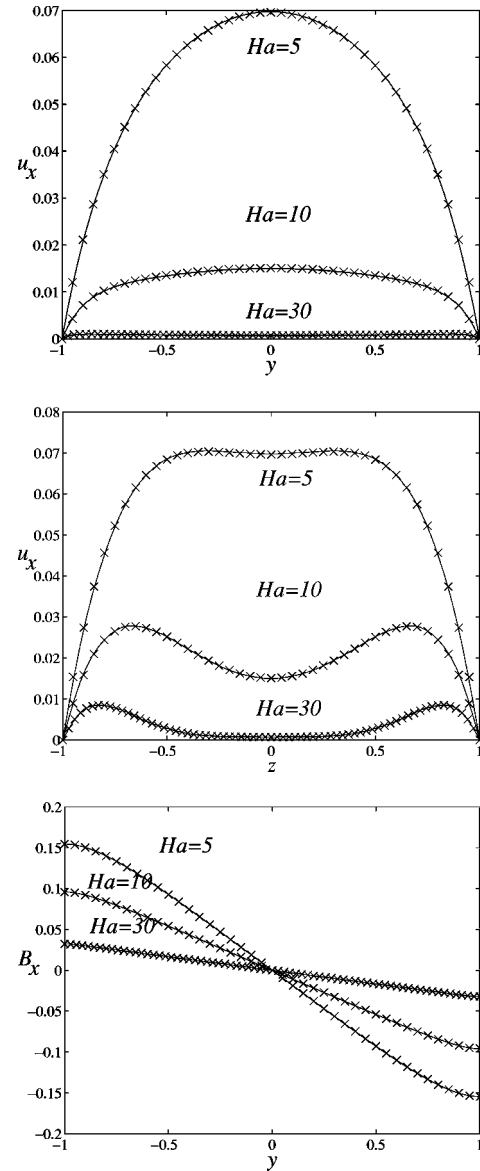

FIG. 4. Velocity profiles and induced magnetic field for various Ha numbers for the case of perfectly conducting Hartmann walls and insulating side walls. Comparison between analytical (solid line) and computational ($\times$) results.

$$\boldsymbol{g}_{j\beta}^{(0)} = W_j[B_\beta + \theta_m^{-1}\boldsymbol{\zeta}_{j\alpha}(u_\alpha B_\beta - B_\alpha u_\beta)], \qquad (9)$$

with α and β standing for the three components of the vector quantities and $\alpha \neq \beta$. The values of θ_m, W_j, and $\boldsymbol{\zeta}_j$ depend upon the choice of the implemented lattice scheme for the magnetic field, which is not necessarily the same as the one for the hydrodynamic flow. The constrains for $\boldsymbol{\zeta}_j$ are $\Sigma_j W_j = 1$ and $\Sigma_j W_j \zeta_{j\alpha}\zeta_{jb} = \theta_m \delta_{ab}$. Furthermore, the lattice has to retain a symmetry up to third order; thus, $\Sigma_j W_j \zeta_{j\alpha} = 0$ and $\Sigma_j W_j \zeta_{j\alpha}\zeta_{j\beta}\zeta_{j\gamma} = 0$ are imposed. Consequently, the required number of discrete velocity vectors for accurate simulations of the magnetic part of the scheme is significantly reduced. The macroscopic quantity of interest is given by $\boldsymbol{B} = \Sigma_j \boldsymbol{g}_j$. In the present work we introduce a 7-bit lattice configuration for the magnetic field, shown in Fig. 1(b), which proves to be

adequate. The corresponding weights are $W_0 = \frac{1}{4}$ and $W_j = \frac{1}{8}$ for $j = 1, 2, 3, 4, 5, 6$ while $\theta_m = 1/4$. The magnetic resistivity is given as $\eta = \tau_m \theta_m \delta t$. This lattice configuration, which we call 3DM7 to distinguish it from the hydrodynamic one, coupled with the 3DQ19 scheme for momentum space maintains high accuracy in all 3D MHD cases tested.

Equations (4) and (8) are implicit but one can circumvent that by introducing [11]

$$\bar{f}_i(\boldsymbol{x},t) = f_i(\boldsymbol{x},t) + \frac{\delta t}{2\tau}[f_i(\boldsymbol{x},t) - f_i^{(0)}(\boldsymbol{x},t)] - \frac{\delta t}{2}\boldsymbol{a}\cdot\boldsymbol{\nabla}_\xi f_i(\boldsymbol{x},t)$$

$$(10)$$

and

$$\overline{\mathbf{g}}_j(\boldsymbol{x},t) = \mathbf{g}_j(\boldsymbol{x},t) + \frac{\delta t}{2\tau_m}[\mathbf{g}_j(\boldsymbol{x},t) - \mathbf{g}_j^{(0)}(\boldsymbol{x},t)]. \qquad (11)$$

Then the discretized evolution lattice kinetic MHD scheme becomes

$$\overline{f}_i(x+\boldsymbol{\xi}_i\delta t, t+\delta t) = \overline{f}_i(x,t) - \frac{\delta t}{(\tau+0.5\delta t)}[\overline{f}_i(x,t) - f_i^{(0)}(x,t)]$$

$$+ \frac{\tau}{(\tau+0.5\delta t)}\boldsymbol{a}\cdot\boldsymbol{\nabla}_{\xi_i}f_i(\boldsymbol{x},t)\delta t, \qquad (12)$$

and

$$\overline{\mathbf{g}}_j(x+\boldsymbol{\zeta}_j\delta t, t+\delta t) = \overline{\mathbf{g}}_j(x,t) - \frac{\delta t}{(\tau_m+0.5\delta t)}[\overline{\mathbf{g}}_j(x,t) - \mathbf{g}_j^{(0)}(x,t)],$$
$$(13)$$

where the equilibrium distributions $f_i^{(0)}$ and $g_j^{(0)}$ are given by Eqs. (5) and (9), respectively, and the forcing term can be computed by Eq. (6), while the macroscopic quantities of interest are given by

$$\varrho = \sum_{i=1}^{N}\overline{f}_i, \quad \varrho\boldsymbol{u} = \sum_{i=1}^{N}\boldsymbol{\xi}_i\overline{f}_i + (\boldsymbol{J}\times\boldsymbol{B})\frac{\delta t}{2}, \quad \boldsymbol{B} = \sum_{j=1}^{M}\overline{\mathbf{g}}_i.$$
$$(14)$$

Equations (12) and (13), along with the use of Eqs. (6) and (14), comprise the implemented LBM algorithm. The current density $\boldsymbol{J} = \boldsymbol{\nabla}\times\boldsymbol{B}$ can be computed either from macroscopic quantities or, more consistently, from higher moments of $\boldsymbol{g}$ [8].

III. RESULTS

The numerical benchmarking of the scheme is accomplished by solving a fully developed MHD flow in a rectangular duct subject to various boundary conditions (Fig. 2). Initially, the magnetic field $\boldsymbol{B}$ is aligned with the y axes. Although the flow is pseudo-2D $[\boldsymbol{u}=(u_x(y,z),0,0)]$, we analyzed fully 3D flow with periodic conditions in the streamwise direction. Both Dirichlet- and Newman-type boundary conditions have been considered. This is one of the few problems of 3D MHD flows where an analytical solution exists [15]. Our numerical results match the corresponding analytical ones with excellent agreement.

Figure 3 depicts the streamwise velocity profiles in the y and z directions for various Hartmann (Ha) numbers, along the corresponding center lines of the duct. In addition, the induced magnetic field component $B_x(y,0)$ is shown. Note that $B_x(0,z)$ is identically equal to zero for the above configuration. Both the side and Hartmann walls are taken to be perfectly insulating. The corresponding results for perfectly conducting Hartmann walls and insulating side walls are shown in Fig. 4. Although the MHD constraint $\boldsymbol{\nabla}\cdot\boldsymbol{B}=0$ is not explicitly imposed, the implemented lattice kinetic scheme fulfills this requirement within machine round-off error. The overall performance of the algorithm and the excellent agreement with analytical results suggest that the present mesoscale kinetic-type approach provides a promising tool in order to tackle complex MHD flows such as plasma and liquid metal flows.

[1] S. Chen and G. D. Doolen, Annu. Rev. Fluid Mech. **30**, 329 (1998).

[2] R. R. Nourgaliev *et al.*, Int. J. Multiphase Flow **29**, 117 (2003).

[3] H. Chen *et al.*, Phys. Fluids **31**, 1439 (1988).

[4] S. Chen, H. Chen *et al.*, Phys. Rev. Lett. **67**, 3776 (1991).

[5] D. O. Martinez *et al.*, Phys. Plasmas **1**, 1850 (1994).

[6] P. Pavlo *et al.*, J. Comput. Phys. **139**, 79 (1998).

[7] A. McNab *et al.* (unpublished).

[8] P. J. Dellar, J. Comput. Phys. **179**, 95 (2002).

[9] F. Bouchut, J. Stat. Phys. **95**, 113 (1999).

[10] N. S. Martys *et al.*, Phys. Rev. E **58**, 6855 (1998).

[11] X. He, S. Chen, and G. D. Doolen, J. Comput. Phys. **146**, 282 (1998).

[12] L. S. Luo, Phys. Rev. E **62**, 4982 (2000).

[13] J. A. McLennan, *Introduction to Non-Equilibrium Statistical Mechanics* (Prentice-Hall, Englewood Cliffs, NJ, 1989).

[14] R. Mei *et al.*, J. Comput. Phys. **161**, 680 (2000).

[15] U. Müller and L. Bühler, *Magnetofluiddynamics in Channels and Containers* (Springer, Berlin, 2001).